euronoise

Pressure fields and their effects in membrane cleaning applications

Fabian Reuter, Robert Mettin and Werner Lauterborn

Göttingen University, Drittes Physikalisches Institut, Friedrich-Hund-Platz 1, 37077 Göttingen, Germany
freuter@physik3.gwdg.de

The ultrasonic field and its cavitation effects are investigated in a membrane module cleaning application. The objective is to derive a better understanding and adaptation of parameters in ultrasonic cleaning baths. Therefore an acoustical model of the membrane module, built up of flat sheet membranes as they are widely used in membrane bioreactors (MBR), is developed to describe the wave propagation. This model could largely be verified by sound pressure measurements on the membrane module and by optical imaging of the cavitation process. Furthermore bubble population and its distribution is characterized and the acoustic pressure measured under variation of parameters, in particular intensity and frequency as well as geometrical parameters.

1 Introduction

In a flexible laboratory setup the ultrasonic (US) cleaning of a submerged polymer membrane module is investigated. This membrane module operates in dead-end filtration and typically finds application in MBRs and in the final purification step in drinking water treatment. To enhance the filtration performance and to reduce facility costs US cleaning during backflushing is a fast in-place cleaning technique and can be successfully applied in polymer membrane cleaning without damaging the membrane [1]. Interactions of microstreamings and collpasing cavitation bubbles with boundaries are mainly responsable for US cleaning. They are induced by the US field, which again monitors bubble oscillations and collapses, e.g. by cavitation noise. So the pressure field should be a good indicator for the cleaning process and is measured by a hydrophone. To distinguish the acoustic pressure radiation sources the pressure field is spectrally evaluated. For further characterization of bubble distribution optical imaging and high speed cinematography are carried out.

2 Experimental arrangement

The investigation is performed on a submerged membrane module made in a downscaled custom-made size. It consists of five stacked flat sheet polymer membranes in A4 format. The membrane sheets are of type UP-150 from Microdyn-Nadir, made from polyethersulfone. Their permeability is specified to 150 kD and they are used in ultrafiltration and microfiltration. The membrane module is submerged into the retentate in a water filled glass container of size $120 \times 50 \times 50$ cm^3. A cake layer on the membrane can be obtained by suction of the permeate from the membranes' inside with controlled transmembrane pressure (TMP) as it determines the cake layer thickness [2]. The cake layer develops on the outside of the membrane and so is observable.
For US generation one or two transducers from Elma, Germany, are submerged into the container. They can run at 35 kHz or 130 kHz in continuous wave or sweep mode with an overall power from 100 W to 2000 W.
The membrane sheets are usually aligned perpendicular to the transducers and the floor, as in the water purification application in MBRs. For imaging the membrane can be rotated around a horizontal axis by 90^o to observe the processes between the membrane sheets. A hydrophone (Reson TC 4038) and a temperature sensor (PT-100) are mounted on a step motor to scan the acoustic pressure together with the temperature in planes. The step motor can be moved in such a way that the pressure field can be measured inside the membrane module between different membrane sheets as well as outside the module. Via a preamplifier (Reson VT 1000), a lowpass with cut-off frequency $f_c = 1.25$ MHz and an oscilloscope (sampling frequency $f_s = 2.5$ MHz) the data are read out with a PC.
Below the membrane module there is a device generating rapidly ascending bubbles from compressed air (≈ 1 bar) overflowing the membranes for removal of disrupted or dissolved filter cake. It is also used to cyclically remove bubbles that adhered to the hydrophone. Additionally, the oxygen content in the water, as an indication of the air content, is measured with an oxymeter. The layout in Fig. 1 gives a side view of the setup.

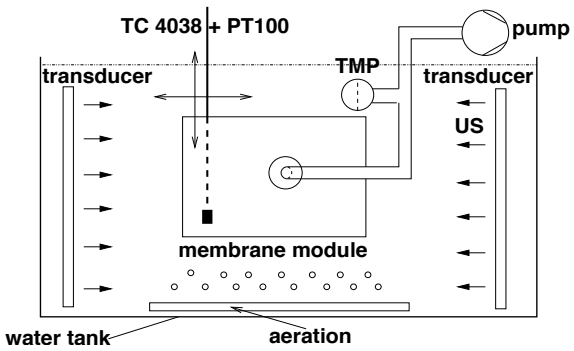

Figure 1: Layout of experimental arrangement.

3 Results

The pressure and temperature field between the membranes and beyond have been measured for different conditions, in particular for two different ultrasonic frequencies (35 kHz and 130 kHz). Strongly different results are found for the two frequencies as well as for the irradiation time and intensity dependence. The temperature measurements show that the water temperature inside the membrane module tends to be lower than outside but strong temperature equalizations in the measured planes occur, attributed to streaming. The overall temperature difference between present bubble structures is below 0.2 °C and rather noisy. Therefore the temperature measurements are not evaluated further here.

3.1 Frequency dependence in propagation behaviour

Previous experiments in a similar arrangement showed successful US cleaning with 130 kHz but no effect with 35 kHz [3]. For good cleaning results the US should

reach the membranes' surface everywhere with the same intensity. So the propagation behaviour through the membrane module is of importance. That is why in the following a simple two-dimensional acoustic model of the membrane module is developed.

3.1.1 Acoustic model of the membrane module

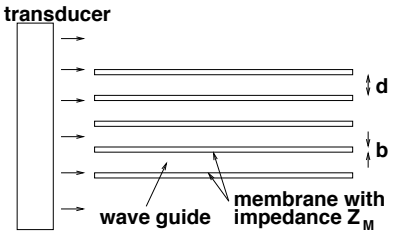

Figure 2: Acoustic model of the membrane module.

Figure 2 shows a sketch of the geometry of the acoustic model in topview. The transducer on the left emits US into the membrane module where the space between the membrane sheets d is considered as a wave guide bounded by the membrane sheets of thickness b and impedance Z_M. To first approximation the membrane can be expected in the following to exhibit soft reflection behaviour while measurements in a Kundt's tube around 35 kHz on a soaked clean membrane show Z_M to be about 10 times lower than the impedance of water. Then due to the boundary condition of vanishing sound pressure on the membranes there is a critical wavelength $\lambda_c = 2d$ for the sound field to propagate [4]. For the critical frequency f_c Eq (1) applies, where c is the sound velocity in water,

$$f_c = \frac{c}{2d}. \qquad (1)$$

At 20 °C and a membrane sheet distance of $d = 8$ mm the critical frequency turns out to be: $f_c = 92.8$ kHz. Starting from this model FEM simulations have been performed for different frequencies. The results are shown in Fig. 3 for $f = 130$ kHz and for $f = 92.4$ kHz, a frequency slightly below the critical frequency. It can be clearly seen that for $f = 92.4$ kHz the sound pressure amplitude decays exponentially within the membrane module while the wave oscillating at $f = 130$ kHz propagates and shows an increase in wavelength between the membranes. Note the pressure maxima due to backscattering on the very left end of the membrane module. Thus a high intensity sound field builds up about one half wavelength in front of the membrane stack.

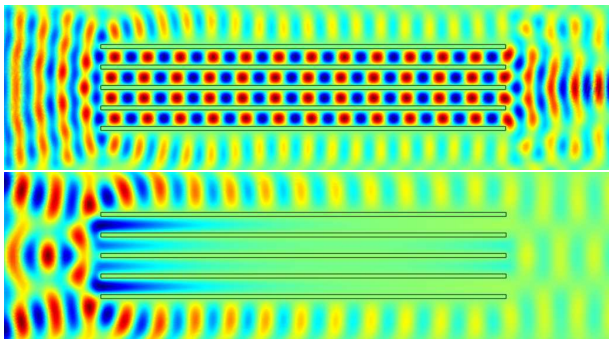

Figure 3: FEM simulation results for the acoustic pressure of the wave guide model with hard reflector on the right and free field condition at the horizontal borders. 130 kHz (top) and 92.3 kHz (bottom).

3.1.2 Sound pressure measurements

Measurements with the hydrophone show that the principal sound field with its characteristic patterns stay amazingly stable for hours. It is further found that without the membrane module in the container a nearly perfect standing wave is formed (not shown here). Thus the difference visible in the acoustic pressure patterns from a perfect standing wave pattern are mainly disturbances caused by the presence of the membrane module. In Fig. 4, with the membrane sheets in the lower right corner, limited by the white lines, the spatial acoustic power distributions are shown for 130 kHz (top) and 35 kHz (bottom). Outside the membrane module standing wave patterns are clearly visible in both images. At 35 kHz the wave does not enter the membrane module at all, even not at very high intensities (not shown here), according to the prediction of Eq (1) from the theoretical model (Fig. 3).

3.1.3 Optical observations

With the naked eye remarkable differences in bubble populations can be observed at different frequencies. Figure 5 compares the bubble populations for 35 kHz and 130 kHz driven with one transducer at 750 mW/cm^2. In the 35 kHz case bubble streamers impinge on the outer membrane surface. They are marked by arrows. Inside the membrane module no bubbles can be per-

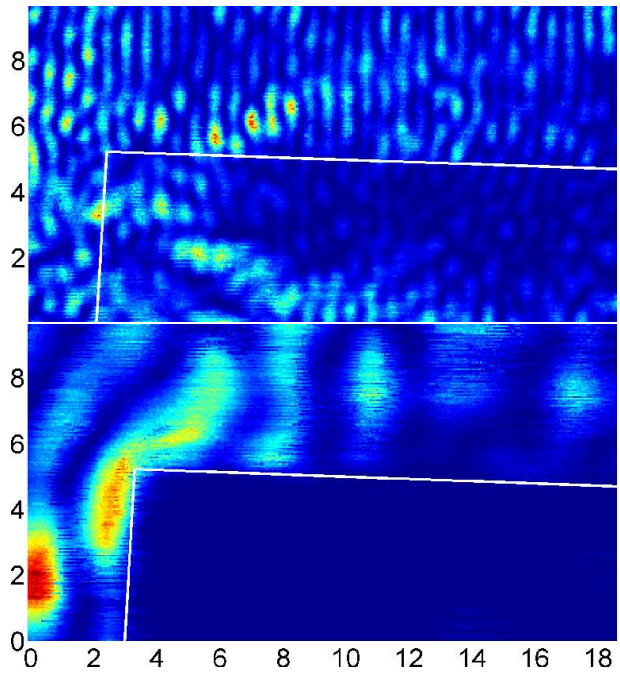

Figure 4: Colour coded acoustical power. Axes in cm. Irradiation with 130 kHz (top) and 35 kHz (bottom) with 75 mW/cm^2 each with one transducer from the left side. The membrane is situated in the lower right corner, limited by the white line.

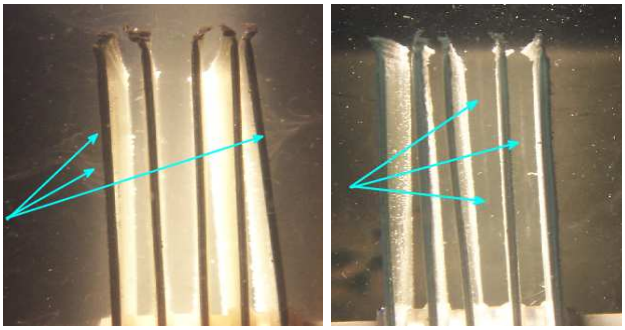

Figure 5: Recording of bubble structures in the membrane module. View from the end of the module towards the transducer. Left 35 kHz, right 130 kHz.

ceived. This situation oughts to have poor cleaning effects and it can be suspected that at high intensities even damage to the outer membranes could be caused. This is in contrast to the situation at 130 kHz where no streamers with directions perpendicular to the membrane surface are visible, but instead bubble layers parallel to the membrane surface between the membrane sheets form (see arrows of the right image of Fig. 5). These bubble layers develop already at low intensities and are supposed to have a significant influence on cleaning efficiency. They are examined more closely by the use of videography in Fig. 6 with the membrane sheets horizontally placed. The image shows a magnified view into one of these bubble layers and the membrane surface at two instants separated by 2 s. The recording is carried out in water of 22 °C with 8.9 mg/l oxygen content. On the lower parts of the videocaptures the membrane with its polymer fibre structure can be well recognized. On its surface several bubbles are located. Their radius is typically in the range of 20 μm to 50 μm, but much bigger bubbles can be found after longer sonication. In the video several bubbles, preferably of size around 25 μm, with potential cleaning effects can be observed: They travel directly along the membrane surface at a speed in the range of 0 to 2.5 cm/s while the liquid streaming velocity even some hundred μm away from the membrane surface does not exceed 0.4 cm/s. So the travelling bubbles on the surface must be driven by acoustic forces. Usually they resettle around existing bubble clusters which therefore have the tendency to grow. However, the surface attached bubbles don't merge, which might be due to repulsive secondary Bjerknes forces at close distance. On the other hand travelling bubbles are also observed to merge with isolated smaller bubbles on the surface that are not arranged into clusters and get carried away subsequently.
The bubble layers parallel to the membrane surfaces shown in the right image of Fig. 5 are vaguely perceptible in the upper right part of the right image of Fig. 6: The blurry white lines are a consequence of light scattered by fast moving bubbles that form the layer.

A closer look reveals that the horizontal speed of the bubbles in the layer rises as a function of increasing distance from the membrane. The travelling bubbles as well as the streaming layer, of course, are shown much more clearly in the corresponding video sequence than in still pictures. Nevertheless, in Fig. 7 a closer look

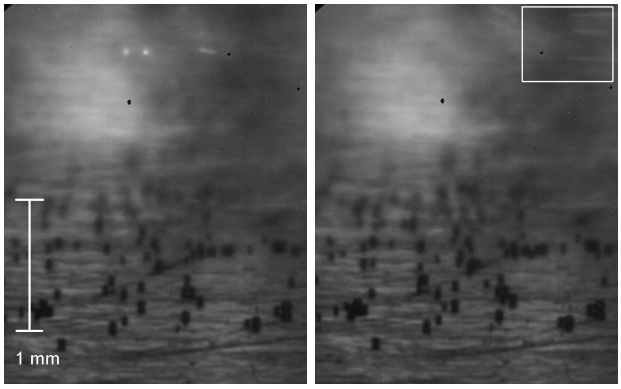

Figure 6: Recording (exposure time 1/60 s) of bubble structures in the membrane module. The right image has been taken 2 s after the left one. A time series of the section within the box is given in Fig. 7.

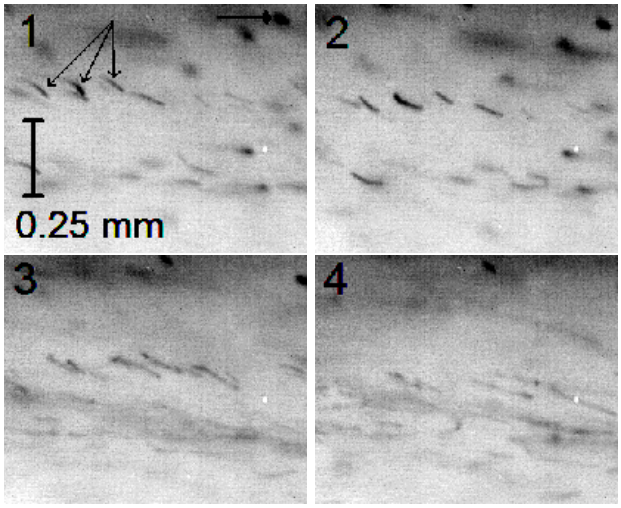

Figure 7: Sequence of images of the bubble layer parallel to membrane sheets. The images are taken 1/600 s one after another (shown in inverted grey scale). $P_e \approx 1.5$ W/cm^2, $f = 130$ kHz.

is taken into the bubble layer. It turns out to consist mainly of two-dimensional streamers. Prerequisite for the occurrence of the streamer structures is the presence of bubble sources [5] which are amply located on the membrane seams and in the water due to dirt particles. Three areas of similar structure are marked by arrows in picture 1. They belong to bubbles or bubble clusters with a radius $r < 5$ μm. Because of the construction of the amplifier feeding the transducer, their speed oscillates strongly with double electric line frequency of 100 Hz from zero up to $v = 2$ m/s for the fastest and around $v = 0.7$ m/s for typically moving bubble structures. Apart from the dominating velocity to the right, away from the closer positioned transducer, they have a net velocity towards the horizontal streaming structure that is visible in the pictures 3 and 4. These two pictures belong to an interval of high power emission from the amplifier. In picture 4 they finally disintegrate or rearrange and interact indistinguishably with the bubbles from the filament in which they merge.
Moreover, there is a particle marked in picture 1 with a round arrow tip. From its velocity the local overall water streaming in the filament can be estimated to

$v_p = 0.08$ m/s. Its motion does not follow the acoustic fluctuations and is rather smooth instead.
Additionally it can be found out from the videocaptures in Fig. 6 that directly after the irradiation with US the bubble density on the surfaces raises by an astoningishly rapid rate of about 20 %/s. It is likely that these bubbles move driven by primary Bjerknes forces from the just mentioned bubble layers of Fig. 7 to the membrane surface after having grown to a certain size in the layer. To estimate this size the same assumptions as in the acoustic model leading to Fig. 3 are made, i.e. , the driving pressure on the membrane surface vanishes. Taking into account the Minnaert frequency, bubbles with a radius bigger than 23 μm should be attracted to the membrane by primary Bjerknes force. This fits well to the minimum bubble radii found on the membrane surface of about 20 μm. It also explains the movement of the three small bubble structures with radii below 1/3 of the Minnaert resonant frequency marked in Fig. 7 towards the antinode into the streaming filament.
The above mentioned processes are best observed in the videos. Because of their size they can only be found on: www.physik3.gwdg.de/∼robert/Conferences.html.
In conclusion thus far poor cleaning effects with 35 kHz can be expected. Therefore only US of 130 kHz will be considered in the following.

3.2 Time dependence

As already mentioned in the context of Fig. 6, the bubble population on the membrane raises rapidly with the onset of US. The bubbles growing on the surface shrink the effective membrane sheet distance d of the wave guide and reduce the critical frequency from Eq (1). Additionally, the bubbles on the membrane sheets can absorb the acoustic power. This can be seen from the upper graph of Fig. 8. It shows the change of the gliding mean of the acoustic power P_{int} in the membrane module that is normalized to its initial value $\langle P_{int} \rangle$. In the first case (red) the acoustic power decreases with time. In the second case (blue) the bubbles from the membrane surface have been removed cyclically by aeration with compressed air. Here the power inside the membrane module stays almost stable with time.

In the lower graph of Fig. 8 the development of the subharmonics (range 1-100 kHz) is plotted. Its strong increase in the case of no aeration seems to be the consequence of big bubbles present at the membrane surface oscillating at small fractions of the driving frequency or subharmonically. So these frequencies are created rather in the module than by transducer.

3.3 Intensity dependence

An increase in irradiation power does necessarily raise the power that is delivered to the membrane module which is available for cleaning. This is shown in Fig. 9, in which the relation between the acoustic power inside the module P_{int} to that outside the module P_{ext} is plotted in dependence on the emitted power P_e, indicating that the efficiency for higher driving powers gets poor.

The sound pressure field at a power of 750 mW/cm^2 is shown in the upper image of Fig. 10 driven with 10 times the power of Fig. 4. The pattern outside the membrane is mainly determined by the distribution of the first harmonic standing wave of 130 kHz. In the membrane module there is only little power. Around the area in front of the membrane where the acoustic model from Fig. 3 predicts intensity peaks due to backscattering, at high intensities different bubble structures occur, like the one marked with the left arrow in the upper image of Fig. 10. According to the decay in the relative acoustic power that reaches the membrane there is a kind of threshold effect for the occurrence of the mentioned structure. This structure begins at the end of a flare structure, described in [6], emitted by the transducer on the left and converts into a filament of smaller bubbles at its tip. The whole structure vanishes after 1-2 cm between the membran sheets. In the lower image only the second harmonic of the upper sound field is shown. From this it can be concluded that in the structure there are bigger bubbles collapsing and soon forming smaller bubbles with higher resonance frequency that travel with streamer direction to the right.

A photo of the structure is shown in Fig. 11. The structure is difficult to observe, so air was injected over the whole transducer surface ten seconds prior to the photo beeing taken. Acoustic measurements show that disturbances of aeration disappear on scales faster than seconds, due to the short transient times in fast cycling sound. The dense mist ahead of the membrane module (left arrow) extending into the gap between the membrane sheets belongs to the structure described above. It differs clearly from the streamers going around the membrane module (right arrow).

So a main reason for this effect seems to be the occurrence of distinct bubble cluster structures at higher intensities just a few centimeters ahead of the membrane module which could absorb the acoustic power and thus acoustically shadow the membrane.

Moreover the observation can be made that at higher intensities the streamers from the surface of the transducer are deflected so that they stream around the mem-

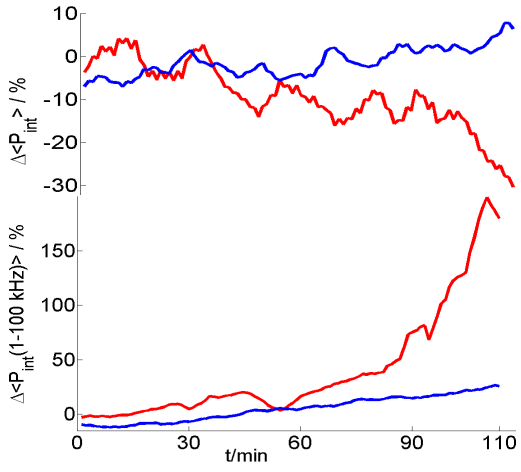

Figure 8: Relative change of normalized power inside the membrane module. Blue with, red without bubble removement. Top: change $\langle P_{int} \rangle$ of overall power, bottom change of $\langle P_{int} \rangle$ in the spectral range 1 kHz - 100 kHz.

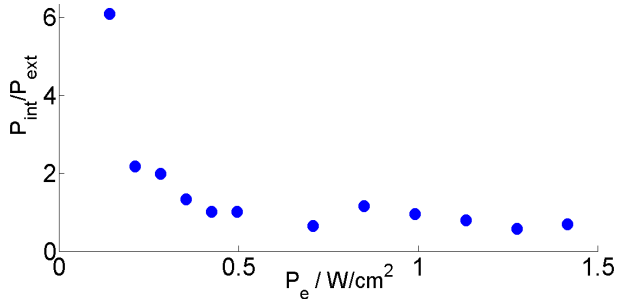

Figure 9: P_{int}/P_{ext} as a function of emitted power P_e.

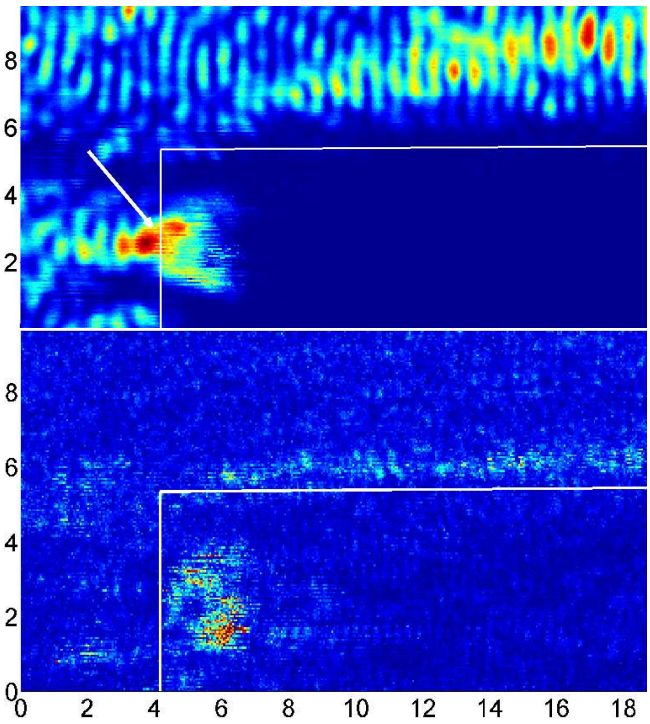

Figure 10: Colour coded acoustical power at 750 mW/cm^2. Axes in cm. The membrane is situated in the lower right corner limited by the white line. Overall power (top) and second harmonic (bottom) are shown in different color scales. The pressure amplitude is up to 3.5 bar.

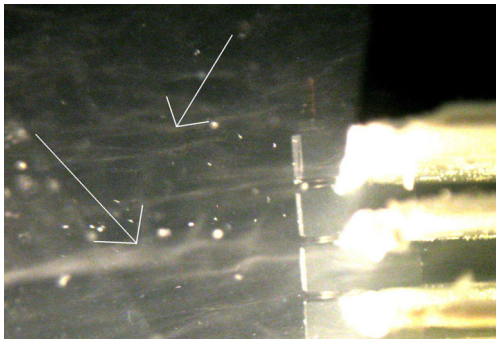

Figure 11: Dense bubble structure (left arrow) ahead of the membrane module, lighter (right arrow) streamers flow around the membrane module. P_e=1.5 W/cm^2, 130 kHz. Measurements of Fig. 10 were carried out between the two lower membrane sheets.

brane module, resulting in a much lower streamer density between transducer and membrane module. This might be caused by the pressure maxima which are repulsive for the streamer bubbles as described in [6]. Operating the system in frequency sweep mode also could not increase the power in the membrane module significantly.
Furthermore it can be seen from the presence of the second harmonic directly above the membrane module (three arrows in Fig. 10) that the membrane seams act as bubble sources and are points of high cavitation activity.

4 Conclusion

Acoustic and optic measurements have been performed at a stack of flat sheet polymer membranes to explain peculiar ultrasonic cleaning results. The sound propagation between the membranes has been calculated (Fig. 3) and measured (Fig. 4 and Fig. 10) for two frequencies (35 kHz and 130 kHz) showing that the low frequency does not propagate into the stack. Consistent with the result is the observation (Fig. 5) that no cavitation is produced between the membranes with the low frequency. This explains why membrane cleaning with a similar stack was not successful at 35 kHz [3]. Stack geometry (distance between membranes) and ultrasonic cleaning frequency are related and must be chosen appropriately. Because of cavitation at higher power input the acoustic field between the membranes depends on the sonication intensity. At higher irradiation intensity the relative internal intensity drops strongly (Fig. 9). This explains the finding that the cleaning showed quite insensitive to the irradiation power, for instance that half the input power gave the same cleaning results [3].

References

[1] S. Lauterborn, W. Urban, "Ultraschallbehandlung getauchter Membranen zur Trinkwasseraufbereitung aus Oberflächenwasser", *7. Aachener Tagung Wasser und Membranen*, W16-1 to W16-12 (2007) (in German)

[2] J. Altmann and Siegfried Ripperger, "Beitrag zur Modellierung der Deckschichtbildung bei der Querstrom-Mikrofiltration", *Chemie Ingenieur Technik 69*, 468-472 (1997) (in German)

[3] S. Lauterborn, W. Urban, "Ultrasonic cleaning of submerged membranes for drinking water applications", this volume

[4] E. Meyer, R. Pottel, Physikalische Grundlagen der Hochfrequenztechnik, *Vieweg Braunschweig*, p. 164 (1969) (in German)

[5] D. Krefting, PhD Thesis, "Untersuchung von Einzel- und Mehrblasensystemen in akustischen Resonatoren", Göttingen (2003) (in German)

[6] R. Mettin, "Bubble structures in acoustic cavitation" in Bubble Dynamics in Acoustic Fields: Modern Trends and Application, A. Doinikov (ed.), *Research Signpost*, pp 1-36 (2005)